Drifter Observations Reveal Intense Vertical Velocity in a Surface Ocean Front

Daniel R. Tarry[1] [ID], **Simón Ruiz[1]** [ID], **T. M. Shaun Johnston[2]** [ID], **Pierre-Marie Poulain[3]** [ID], **Tamay Özgökmen[4]** [ID], **Luca R. Centurioni[2]**, **Maristella Berta[5]** [ID], **Giovanni Esposito[5]** [ID], **J. Thomas Farrar[6]** [ID], **Amala Mahadevan[6]**, and **Ananda Pascual[1]** [ID]

[1]IMEDEA (CSIC-UIB), Esporles, Spain, [2]Scripps Institution of Oceanography, University of California, San Diego, La Jolla, CA, USA, [3]NATO-STO-CMRE, La Spezia, Italy, [4]University of Miami, Miami, FL, USA, [5]Consiglio Nazionale delle Ricerche - Istituto di Scienze Marine, Lerici, Italy, [6]Woods Hole Oceanographic Institution, Woods Hole, MA, USA

Abstract Measuring vertical motions represent a challenge as they are typically 3–4 orders of magnitude smaller than the horizontal velocities. Here, we show that surface vertical velocities are intensified at submesoscales and are dominated by high frequency variability. We use drifter observations to calculate divergence and vertical velocities in the upper 15 m of the water column at two different horizontal scales. The drifters, deployed at the edge of a mesoscale eddy in the Alboran Sea, show an area of strong convergence ($\mathcal{O}(f)$) associated with vertical velocities of -100 m day^{-1}. This study shows that a multilayered-drifter array can be an effective tool for estimating vertical velocity near the ocean surface.

Plain Language Summary The study of vertical motions in the ocean is a key challenge as they are difficult to measure and predict although their impact is crucial on the exchange of water properties in the water column. Here, we use high resolution drifter observations to calculate vertical velocities in the upper layers of a surface density front. This study shows high values of downward speed combined with a high temporal variability at the surface layer.

1. Introduction

Mesoscale (10–100 km) vertical motions are typically 3–4 orders of magnitude smaller than the horizontal velocities and lie at the edge of our observational capabilities. In submesoscale flows, with horizontal scales smaller than 10 km and a time duration from hours to days (Charney, 1971; McWilliams, 2016), the flow departs from geostrophic balance in the presence of strong lateral buoyancy gradients with Rossby (R_o) number around 1. The calculation of w at these scales represents a challenge due to the lack of high-resolution data and only vertical velocities associated with strong submesoscale processes (<1 km) are intense enough to be measured (D'Asaro et al., 2018; Tarry et al., 2021). Surface frontal regions develop ageostrophic secondary circulations that lead to strong surface convergence of $\mathcal{O}(f)$, where f is the Coriolis frequency, and intense vertical velocities of $\mathcal{O}(100)$ m day^{-1} (Capó et al., 2021; Freilich & Mahadevan, 2019; Lévy et al., 2001; Mahadevan & Archer, 2000; Mahadevan et al., 2016; McWilliams, 2016; McWilliams et al., 2019; Tarry et al., 2021).

The Alboran Sea, located in the westernmost part of the Mediterranean Sea, provides an ideal scenario to measure vertical velocities. Sharp surface density fronts are created when the inflowing Atlantic waters meet the denser Mediterranean waters (Allen et al., 2001; Pascual et al., 2017; Tintoré et al., 1988). Several studies have performed estimations of vertical velocities previously in this region (Table 1). However, most of these studies focused on motion in the pycnocline, below the mixed layer. Observational studies used quasi-geostrophy (QG) to estimate vertical velocities, ranging from 10 to 75 m day^{-1}. On the other hand, the vertical velocities obtained from models show a wide range of magnitude. Very recently, Tarry et al. (2021) used in situ observations to calculate vertical velocities in the surface layer and obtained values of 100 m day^{-1} from drifter-computed divergence and 800 m day^{-1} measured by a neutrally buoyant Lagrangian float designed to follow the 3-D motion of water. These large values of w are sporadic events over limited depths and areas of the ocean.

In this study, we use clusters of surface and near-surface drifters to calculate horizontal divergence and vertical vorticity. Then we use two different methods to calculate the vertical velocity at different horizontal scales. Observations from drifter clusters have proven to be especially useful to characterize the velocity gradients at several scales (Berta et al., 2016, 2020; D'Asaro et al., 2018; Esposito et al., 2021; Ohlmann et al., 2017; Poje

Table 1
Vertical Velocity Values From Previous Studies in the Alboran Sea

	w (m day^{-1})	Method	Scale	Depth (m)
Tintoré et al. (1991)	75	QG	50 km	100
Flexas et al. (2006)	15	QG	30–40 km	75
Allen et al. (2001)	20	QG	20 km	50–100
Ruiz et al. (2019)	10	QG	20 km	50
Gomis et al. (2001)	45	QG	20 km	77
Ruiz et al. (2019)	20	Model	<10 km	50
Capó et al. (2021)	1,000	Model	<10 km	125
Freilich and Mahadevan (2021)	30–40	Model	<10 km	40
Tarry et al. (2021)	100	Drifters	<10 km	10
Tarry et al. (2021)	800	Float	<10 m	1–10

et al., 2014; Poulain et al., 2021). The high-frequency sampling of the drifters provides a detailed time series of vertical velocity in the upper 15 m along a front located at the edge of a mesoscale eddy. In Section 2, we describe the data and methods used. In Section 3, we present and discuss the results obtained and in Section 4, we conclude our analysis.

2. Data and Methods

The data used in this work were obtained during the second cruise of the CALYPSO project (Coherent Lagrangian Pathways from the Surface Ocean to Interior) (Mahadevan et al., 2020). The cruise took place between 27 March and 10 April 2019 in the Alboran Sea, the westernmost basin in the Mediterranean Sea, on board the RV *Pourquoi Pas?*.

2.1. Drifter Data

In the early morning of April 5, an array formed by 30 drifters was deployed in about 2 hr in the eastern side of an anticyclonic gyre located near the south coast of Spain (Figure 1). The drifter array was composed of 15 surface drifters (CARTHE) and 15 near-surface drifters (SVP). The CARTHE drifter consists of a buoy attached to a drogue that extends 60 cm below the surface; designed to be eco-friendly (85% biodegradable), compact, and low cost (Novelli et al., 2017), it is optimal for large array deployments (D'Asaro et al., 2018; Haza et al., 2016; Mahadevan et al., 2020). The SVP drifter is the standard drifter of the Global Drifter Program (Centurioni, 2018; Lumpkin & Pazos, 2007; Niiler, 2001; Sybrandy & Niiler, 1991). It is a surface buoy attached to a holey sock drogue that tracks the horizontal motion of water at a depth of 15 m. Drifters transmitted their GPS position every 5 min as they went south following the gyre circulation.

2.2. Underway CTD Data

The Underway CTD (UCTD) is a profiling instrument that is used to measure seawater conductivity, temperature, and pressure (Rudnick & Klinke, 2007) while the ship is underway. Repeated vertical profiles of the upper 200–250 m of temperature (T) and salinity (S) were collected across the anticyclonic gyre (Figure 1) with a horizontal resolution of about 1 km and vertically gridded into 0.5 m bins.

2.3. Kinematic Properties and Vertical Velocity Estimation

Several studies have used the two-dimensional velocity gradients to express the kinematic properties of the flow (Kirwan, 1975; Molinari & Kirwan, 1975; Okubo, 1970; Okubo & Ebbesmeyer, 1976). Following the naming convention (e.g., Kirwan, 1975), we define the horizontal divergence, vertical vorticity, and shear and normal strain rates as $\delta = u_x + v_y$, $\zeta = v_x - u_y$, and $\sigma_s = v_x + u_y$ and $\sigma_n = u_x - v_y$, respectively. We combine shearing and normal strain into strain rate $\sigma = \sqrt{\sigma_s^2 + \sigma_n^2}$. Hereafter, unless noted, the term "divergence" will refer to the
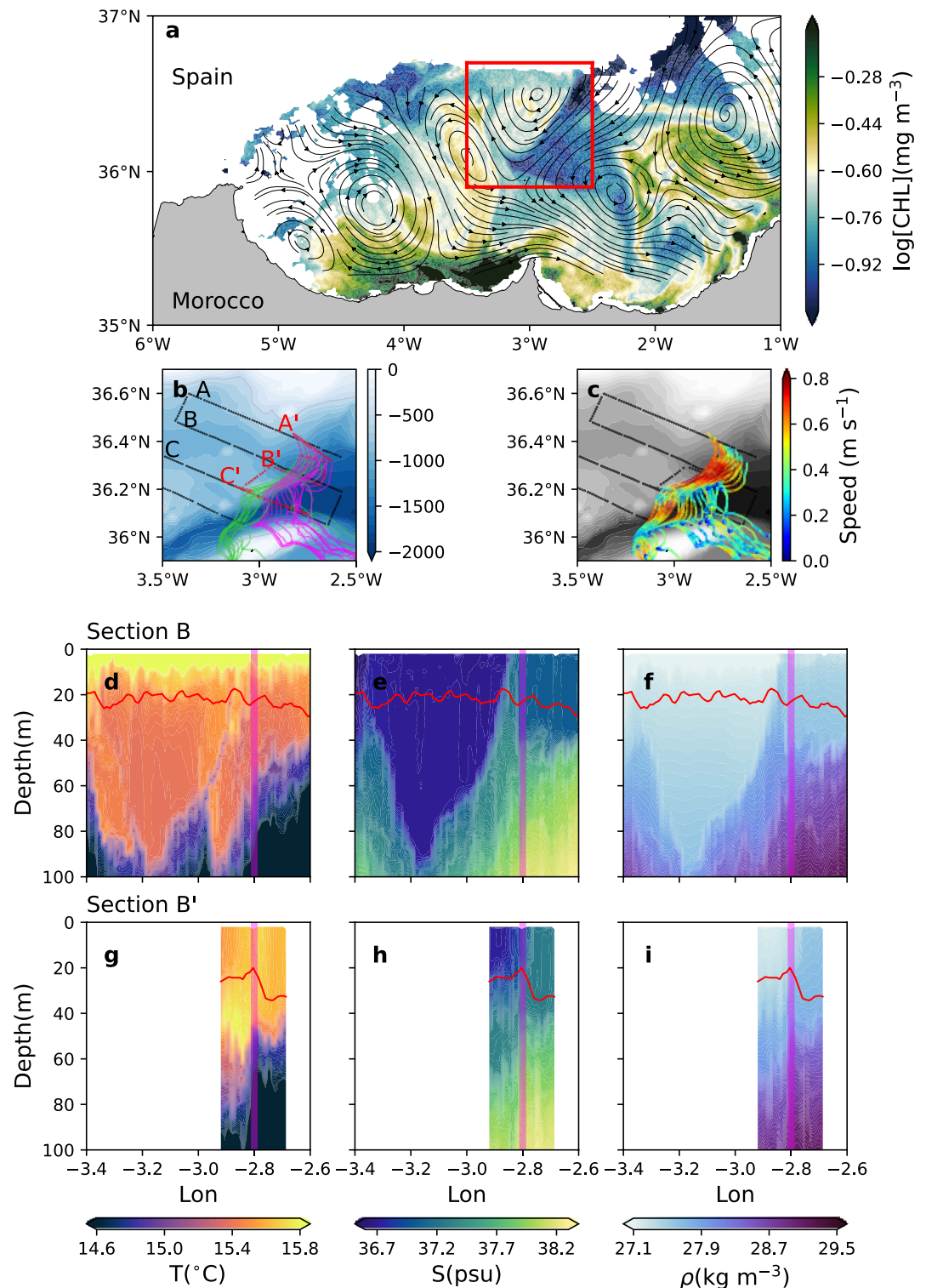
Figure 1. (a) Chlorophyll concentration in the Alboran Sea for 1 April 2019 with stream function contours from absolute dynamic topography. The red box indicates the region shown in panels (b and c). (b) Three-day trajectories for the drifters deployed on 5 April 2019. Pink trajectories are for the surface drifters while the green ones are for the near-surface drifters. A dotted line shows the Underway CTD (UCTD) sampling with each zonal section labeled. Bathymetry is plotted in the background. Panel (c) same as (b) but with drifter velocities. (d–f) UCTD vertical sections of conservative temperature, absolute salinity, and potential density, respectively, for transect B in panel (b). Panels (g–i) same as (d–f) but for transect B′. Red solid line shows the mixed layer depth computed from the density profiles.

horizontal divergence normalized by the Coriolis frequency f, the "vorticity" to the vertical vorticity normalized by f, and the "strain" to the strain rate normalized by f.

Here, we use the method proposed by Molinari and Kirwan (1975), a two-dimensional linear least squares fit, to compute the kinematic properties of the flow from drifter observations. We obtain cluster-averaged kinematic properties from the computed velocity gradients for all available clusters formed by six drifters following Tarry et al. (2021) and (Essink et al., 2022). The standard deviation of the kinematic properties decreases with number of drifters per cluster (Molinari & Kirwan, 1975) and the error due to GPS uncertainty is inversely proportional to the number of drifters (Spydell et al., 2019). Hence, using six drifters per cluster is a good compromise between increasing the method's accuracy and still having sufficient clusters. The total number of clusters is given by all combinations of six drifters without repetitions (Tarry et al., 2021). The length scale L and the aspect ratio α are also relevant for the accuracy in the velocity gradient estimate. The length scale of the cluster is important since this method was devised for small separation distances and/or a linear velocity field (Molinari & Kirwan, 1975). We define the length scale of a cluster as the root mean squared distance of all pairs of drifters. The aspect ratio defines the regularity of a cluster and is represented as the quotient between the minor and major eigenvalues of the position covariance matrix, $\alpha = \lambda_{\min}/\lambda_{\max}$ (Choi et al., 2017). Regular clusters will have an aspect ratio of one, while elongated clusters will have an aspect ratio close to zero and will produce velocity gradient estimates with a low correlation with respect to the actual velocity field. To remove inaccurate estimates arising from an uneven description of the two-dimensional flow field, we remove any elongated clusters from the analysis. Essink et al. (2022) found this threshold to be 0.1. Focusing on the submesoscale, divergence and vorticity values were calculated every 15 min for the first 12 hr after the deployment.

The vertical motion can be estimated from the continuity equation, $u_x + v_y + w_z = 0$, where u, v, and w are the zonal, meridional, and vertical velocities, respectively. Here, x, y are the horizontal coordinates and z is the vertical coordinate. The continuity equation relates the horizontal convergence ($u_x + v_y < 0$) with divergence in the vertical ($w_z > 0$), for example, at the surface ocean (where $w \sim 0$), this would imply downwelling that decreases in magnitude as depth increases. It is possible to estimate w at any desired depth level by vertically integrating the continuity equation from some reference level, where w is known

$$w(z = h_1) - w(z = h_2) = -\int_{z=h_2}^{z=h_1} (u_x + v_y)\, dz. \tag{1}$$

Since w at the surface is approximately zero, Equation 1 can be reduced to

$$w(z = -h) = \int_{-h}^{0} (u_x + v_y)\, dz, \tag{2}$$

where h is the integration depth (positive). To use Equation 2 we need to know the vertical distribution of the horizontal divergence. As we have drifters at two different depths, we can fit a linear profile from the drifter-computed divergence. Equation 2 can be simplified into Equation 3 if the horizontal divergence is assumed to be depth independent in the mixed layer (Poulain, 1993). With this equation, we can use the SVP-computed divergence to calculate w at 15 m depth.

$$w(h) = h\,(u_x + v_y). \tag{3}$$

When computed from observational data, the w values obtained are subject to a number of uncertainties that arise from observational errors, uncertainties in the least squares method or the linear fit of the horizontal divergence. The propagation of position uncertainties due to GPS error ($\sim$5 m) yields estimates of the velocity errors of $\sim$0.01 m/s (Centurioni, 2018; Hormann et al., 2016; Maximenko et al., 2013). Spydell et al. (2019) and Tarry et al. (2021) estimated the uncertainty in the least squares method to be the 10% of the kinematic property value.

3. Results and Discussion

On 1 April 2019, satellite absolute dynamic topography (ADT) indicated the presence of an anticyclonic eddy in the northern Alboran Sea, near the south coast of Spain (Figure 1a). ADT and sea surface chlorophyll concentration maps indicate that the eddy had a surface extension of about 50 km. On the eastern side, the edge of the eddy is marked by a sharp horizontal gradient on chlorophyll. These low chlorophyll waters follow the circulation
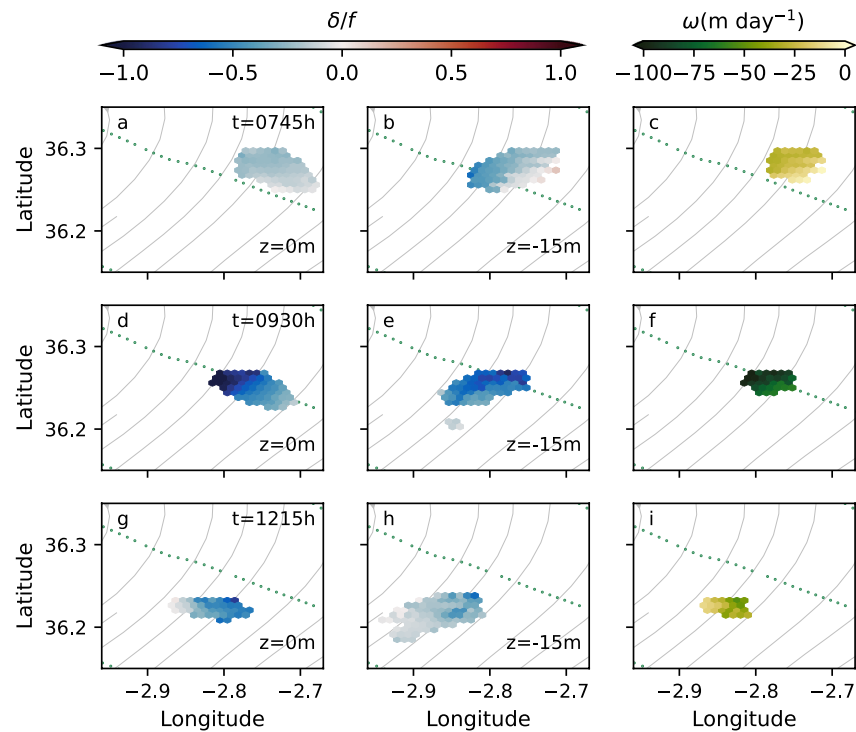
Figure 2. Composite spatial maps hours after the deployment (5 April 2019). Drifter-computed divergence at (a, d, and g) $z = 0$ m, and (b, e, and h) $z = -15$ m. Maps show the median value of latitude-longitude hexagonal bins (0.5-km radius) containing more than 10 data points. (c, f, and i) Vertical velocity calculated at $z = -15$ m from common bins between surface and 15 m depth. The green dotted line indicates the Underway CTD sampling line B. Stream function contours derived from absolute dynamic topography are plotted in the background.

creating a filament that goes around the eddy. The drifter array was deployed on the eastern side, where the horizontal gradients were stronger (Figure 1b). They traveled through the edge of the eddy at a speed of 0.6–0.8 m/s (Figure 1c) and then separated at the southernmost point. The first leg of UCTD sampling across the gyre (black dotted line in Figure 1b) shows the hydrographic structure and revealed a clear frontal region which extended far below the mixed layer depth (Figures 1d–1f). The waters inside the gyre are characterized by the low salinity of the relatively fresh Atlantic waters, which are significantly less dense than the resident Mediterranean waters. The signature of the gyre reaches the 100 m depth. The stronger horizontal gradients are located at the eastern side of the gyre, matching the chlorophyll satellite observations. The front is mainly driven by a salinity difference as can be seen by comparing Figures 1d and 1e. In fact, Figure 1d shows a tongue of surface warm water being subducted in the frontal region (at about 2.75°W). The second leg of UCTD sampling (red dotted line in Figure 1b), despite covering a smaller section, shows an eastward displacement of the frontal region.

The drifter-computed divergence for clusters with a length scale smaller than 10 km is plotted in spatial binned maps in Figures 2c, 2f, and 2i. The left and middle column panels show divergence computed from surface and 15-m clusters respectively. We use the median as aggregation method within the bins instead of the mean to minimize the effect of extreme values in the distribution of the data. As can be seen, for the same time step, there is correspondence between the surface and 15 m divergence. Both sets of drifters converge as they travel along the front. The maximum convergence over the first 12 hr after the deployment happen at April 5 9:30 hr, when the drifters cross over the subduction seen in the UCTD vertical sections (Figures 1d–1i). At this point, we obtain convergence values of $\mathcal{O}(f)$ at the surface and 15 m depth (Figures 3a–3d). At both depths, the stronger convergence is obtained from the smaller scale clusters (∼5 km) and are associated with a weak signal in vorticity ($\pm 0.1\ f$) (Figures 3e–3h).

In addition, we can gain further information on the properties of the flow if we plot the divergence of the 12 hr analysis in the vorticity-strain plane (Figure 4). In this plane, the flow regime can be decomposed into three regions: The anticyclonic vorticity-dominated (AVD) region ($\zeta < 0$ and $\sigma < |\zeta|$), the strain-dominated (SD) region
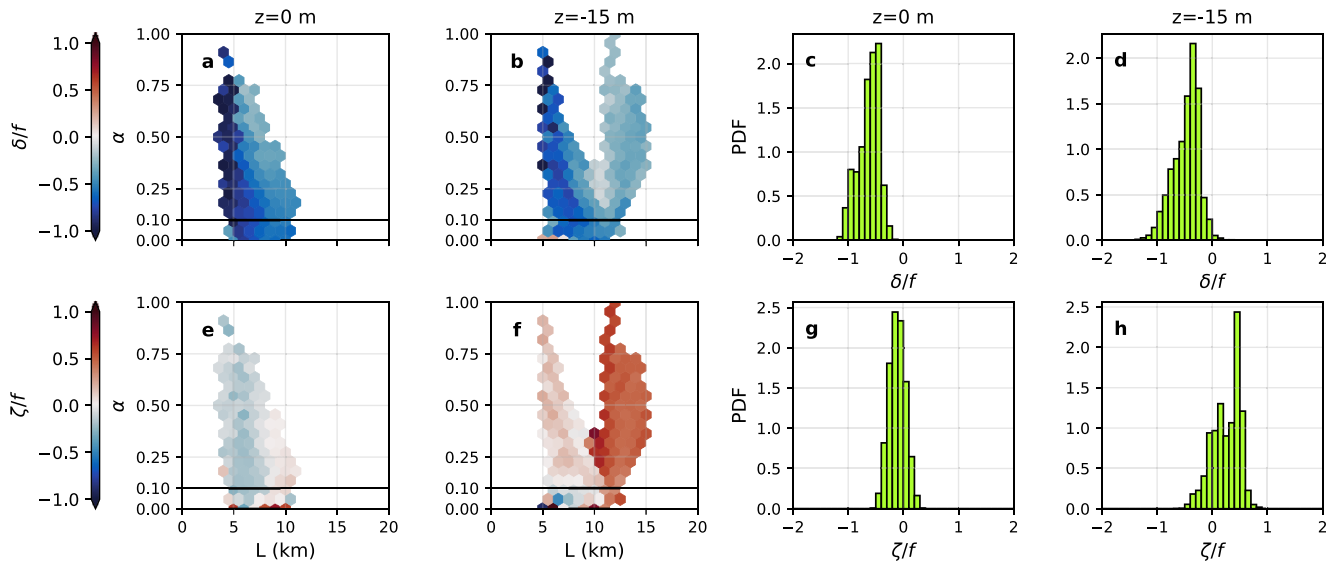
Figure 3. (top row) Divergence and (bottom row) vorticity at 9:30 hr 5 April 2019 (when w is maximum). (a, b, e, and f) Median values of length scale-aspect ratio hexagonal bins containing more than 10 data points. The solid line at $\alpha = 0.1$ delimits the boundary below the clusters that are too elongated to be considered. (c, d, g, and h) Histograms of divergence and vorticity; only the values from clusters with $\alpha \geq 0.1$ are counted. Panels (a, c, e, and g) show the kinematic properties at the surface while panels (b, d, f, and g) at the 15 m depth.

($\sigma \geq |\zeta|$), and the cyclonic vorticity-dominated (CVD) region ($\zeta > 0$ and $\sigma < |\zeta|$). Fronts prone to generate intense vertical velocities at the surface will have vorticity and strain values that lie above the $\sigma = |\zeta|$ lines, at a distance that is determined by the strength of the surface divergence (Balwada et al., 2021; Shcherbina et al., 2013). As expected, the bulk of the clusters fall into the strain dominated (SD) region ($\sigma > |\zeta|$), which confirms the strain dominance in the front. The stronger values of convergence at surface are within the $\sigma = \sqrt{2}|\zeta|$ lines. Here, the divergence is equal in magnitude with the vorticity and strain (i.e., $|\delta| \sim |\zeta| \sim |\sigma|$). On the other hand, at a 15-m depth, the stronger convergence is associated with low values of vorticity, meaning that the flow regime is dominated by the strain.

Making use of Equation 2, we calculate w for the horizontally colocated bins in a given time step (Figures 2c, 2f, and 2i). This condition ensures that the divergence considered at the surface and 15 m depth when applying Equation 2 has the same location, reducing spurious w estimates due to spatial variability on δ. This condition is

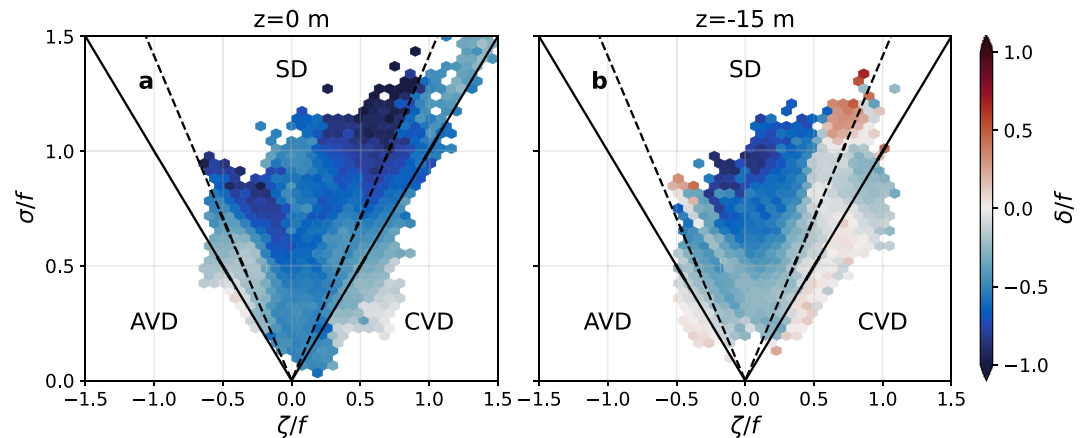**Figure 4.** Divergence median values of vorticity-strain hexagonal bins containing more than 10 data points over the first 12 hr after the deployment. The solid lines are the $\sigma/f = |\zeta|/f$ lines, which delimit the boundaries between the anticyclonic vorticity-dominated (AVD), strain-dominated (SD), and cyclonic vorticity-dominated (CVD) regions. The dashed lines are the $\sigma/f = \sqrt{2}|\zeta|/f$ lines.
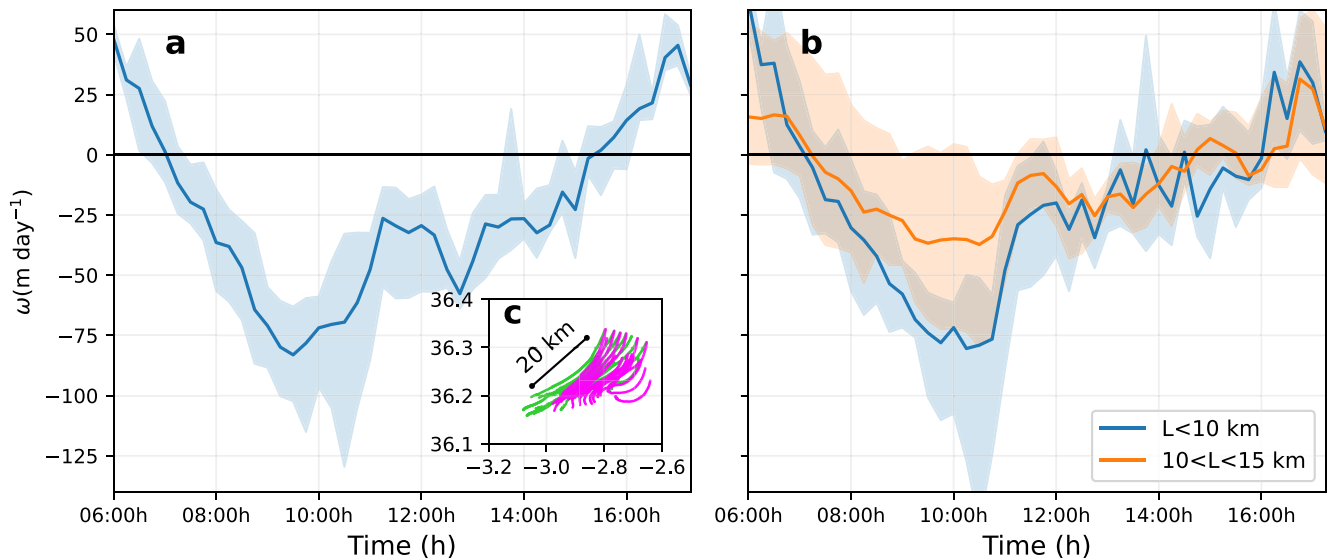
Figure 5. Time series of w integrated at $z = -15$ m from drifter-calculated divergence using (a) Equation 2 and (b) Equation 3 during 5 April 2019. The thick line indicates the median value for all the bins available at each time step and the shading indicates the 95% confidence intervals. In panel (b) the blue solid line shows the w obtained from clusters smaller than 10 km and the orange solid line from clusters between 10 and 15 km. (c) Twelve-hour trajectories of the surface (pink) and near-surface (green) drifters.

what limits our analysis to a 12-hr long time series, as after this time, the surface and near-surface drifters drift away (Figure 1). Applying this method to all the analysis outputs with $L < 15$ km, we obtain a 12-hr long Lagrangian time series of w along the front with a time resolution of 15 min (Figure 5a). During this time, the drifters travel a distance of approximately 20 km along the front (Figure 5c). At first glance, the time series shows a rapid variability of w in the first 15 m; starting with positive values in the early moments after the deployment followed by an immediate switch to negative values. The maximum downward speed obtained reaches 100 m day^{-1} and coincides in space with the subduction observed in the vertical section of the UCTD sampling (Figure 2f). Over 4 hr, w along the front varies a total of 150 m day^{-1}. The error on these estimates were calculated by propagating the error on the surface and 15 m divergences, obtaining an error of the 20% of the signal. From the dynamical point of view, the rapid variability of w could be related to different mechanisms. Episodes of frontogenesis and development of ageostrophic secondary circulations with resting or relaxation phases can lead to such variability (Capó et al., 2021). Another option is that we could be seeing the signature of an internal wave. In this case, this vertical displacement would not translate into vertical net flux. Oscillating divergence signals of $\mathcal{O}(f)$ have been observed, including in the earliest estimates from drifters (Molinari & Kirwan, 1975). With such a short time series nor additional data from other platforms, it is not possible to clarify which is the mechanism responsible for the high variability of the vertical velocity.

The larger dispersion of the near-surface drifters (Figures 3b and 3d) allows us to calculate w at larger scales ($10 < L < 15$ km) (Figure 5b). $w_{<10\,\text{km}}$ is calculated from clusters that satisfy the condition $L < 10$ km while $w_{>10\,\text{km}}$ uses clusters with $10 < L < 15$ km. Since there are not enough surface clusters at this scale, we make use of Equation 3 to calculate w. As a validation method, we also calculate $w_{<10\,\text{km}}$ using Equation 3 and see that we obtain similar time series with the two methods. In this case, the depth independent divergence assumption is a good approximation as both layers experience the same order of convergence (Figures 3e and 3f). The results in Figure 5b show that $w_{<10\,\text{km}}$ exceeds $w_{>10\,\text{km}}$ by a factor of 2 at the time of the maximum downward speed. This result shows a scale dependence of w and reemphasizes the role played by the smaller scales in the vertical flow field (Balwada et al., 2021; Esposito et al., 2021; Ohlmann et al., 2017; Poulain, 1993; Ruiz et al., 2019; Tarry et al., 2021; Yu et al., 2019).

4. Conclusion

We provide a high frequency time series of submesoscale w derived from drifter observations in a surface frontal region in the Alboran Sea. The drifter-computed divergence showed a strong convergence of $\mathcal{O}(f)$ in the upper

15 m leading to maximum downward speeds of 100 m day^{-1}. At the same location, the temperature profiles from the UCTD sampling across-front suggested the subduction of warm surface waters down to 40 m. w along the front showed a high temporal variability, ranging from 50 m day^{-1} to -100 m day^{-1} in less than 4 hr. The maximum downwelling was observed in the subduction region. Finally, we analyzed the horizontal scale dependence using clusters with different length scale. The results showed that, at the point of maximum downward speed, $w_{<10 \text{ km}}$ exceeded $w_{>10 \text{ km}}$ by a factor of 2.

The capability of drifters to capture small localized submesoscale events of short duration but high intensity has already been reported previously (D'Asaro et al., 2018; Tarry et al., 2021). These studies mainly used drifters to determine regions of surface convergence. Here, we go a step forward and demonstrate that the deployment of multilayered-drifter arrays is a useful asset to estimate w at a high resolution at the surface layers of the water column. The separation of the contribution of submesoscale variability and internal waves to w represents a further challenge and needs additional analysis, as well as complementary data from other platforms and a longer time series of w, and shall be focused on future studies. More work is needed to retrieve information from the submesoscale vertical processes from multilayer drifter deployments.

Data Availability Statement

Remotely sensed sea level anomaly and sea surface chlorophyll concentration came from Copernicus Marine Environment Monitoring Service (CMEMS). European Ocean Gridded L4 Sea Surface Heights and derived variables nrt (https://doi.org/10.48670/moi-00142). European Sea Surface Chlorophyll Concentration from Multi Satellite observations (https://doi.org/10.48670/moi-00095). The drifter and UCTD data sets used are available at https://doi.org/10.5281/zenodo.6473661.

References

Allen, J. T., Smeed, D. A., Tintoré, J., & Ruiz, S. (2001). Mesoscale subduction at the Almeria–Oran front: Part 1: Ageostrophic flow. *Journal of Marine Systems*, *30*(3), 263–285. https://doi.org/10.1016/S0924-7963(01)00062-8

Balwada, D., Xiao, Q., Smith, S., Abernathey, R., & Gray, A. R. (2021). Vertical fluxes conditioned on vorticity and strain reveal submesoscale ventilation. *Journal of Physical Oceanography*, *51*(9), 2883–2901. https://doi.org/10.1175/JPO-D-21-0016.1

Berta, M., Griffa, A., Haza, A. C., Horstmann, J., Huntley, H. S., Ibrahim, R., et al. (2020). Submesoscale kinematic properties in summer and winter surface flows in the Northern Gulf of Mexico. *Journal of Geophysical Research: Oceans*, *125*(10), e2020JC016085. https://doi.org/10.1029/2020JC016085

Berta, M., Griffa, A., Özgökmen, T. M., & Poje, A. C. (2016). Submesoscale evolution of surface drifter triads in the Gulf of Mexico. *Geophysical Research Letters*, *43*(22), 11751–11759. https://doi.org/10.1002/2016gl070357

Capó, E., McWilliams, J. C., Mason, E., & Orfila, A. (2021). Intermittent frontogenesis in the Alboran Sea. *Journal of Physical Oceanography*, *51*(5), 1417–1439. https://doi.org/10.1175/JPO-D-20-0277.1

Centurioni, L. R. (2018). Drifter technology and impacts for sea surface temperature, sea-level pressure, and ocean circulation studies. In R. Venkatesan, A. Tandon, E. D'Asaro, & M. A. Atmanand (Eds.), *Observing the oceans in real time* (pp. 37–57). Springer International Publishing. https://doi.org/10.1007/978-3-319-66493-4_3

Charney, J. G. (1971). Geostrophic turbulence. *Journal of the Atmospheric Sciences*, *28*(6), 1087–1095. https://doi.org/10.1175/1520-0469(1971)028<1087:gt>2.0.co;2

Choi, J., Bracco, A., Barkan, R., Shchepetkin, A. F., McWilliams, J. C., & Molemaker, J. M. (2017). Submesoscale dynamics in the northern Gulf of Mexico. Part III: Lagrangian implications. *Journal of Physical Oceanography*, *47*(9), 2361–2376. https://doi.org/10.1175/jpo-d-17-0036.1

D'Asaro, E. A., Shcherbina, A. Y., Klymak, J. M., Molemaker, J., Novelli, G., Guigand, C. M., et al. (2018). Ocean convergence and the dispersion of flotsam. *Proceedings of the National Academy of Sciences*, *115*(6), 1162–1167. https://doi.org/10.1073/pnas.1718453115

Esposito, G., Berta, M., Centurioni, L., Johnston, T. S., Lodise, J., Özgökmen, T., et al. (2021). Submesoscale vorticity and divergence in the Alboran Sea: Scale and depth dependence. *Frontiers in Marine Science*, *8*, 843. https://doi.org/10.3389/fmars.2021.678304

Essink, S., Hormann, V., Centurioni, L. R., & Mahadevan, A. (2022). On characterizing ocean kinematics from surface drifters. *Journal of Atmospheric and Oceanic Technology*, *39*(8), 1183–1198. https://doi.org/10.1175/JTECH-D-21-0068.1

Flexas, M., Gomis, D., Ruiz, S., Pascual, A., & León, P. (2006). In situ and satellite observations of the eastward migration of the Western Alboran Sea Gyre. *Progress in Oceanography*, *70*(2), 486–509. https://doi.org/10.1016/j.pocean.2006.03.017

Freilich, M. A., & Mahadevan, A. (2019). Decomposition of vertical velocity for nutrient transport in the upper ocean. *Journal of Physical Oceanography*, *49*(6), 1561–1575. https://doi.org/10.1175/jpo-d-19-0002.1

Freilich, M. A., & Mahadevan, A. (2021). Coherent pathways for subduction from the surface mixed layer at ocean fronts. *Journal of Geophysical Research: Oceans*, *126*(5), e2020JC017042. https://doi.org/10.1029/2020JC017042

Gomis, D., Ruiz, S., & Pedder, M. (2001). Diagnostic analysis of the 3D ageostrophic circulation from a multivariate spatial interpolation of CTD and ADCP data. *Deep Sea Research Part I: Oceanographic Research Papers*, *48*(1), 269–295. https://doi.org/10.1016/S0967-0637(00)00060-1

Haza, A., Özgökmen, T., & Hogan, P. (2016). Impact of submesoscales on surface material distribution in a Gulf of Mexico mesoscale eddy. *Ocean Modelling*, *107*, 28–47. https://doi.org/10.1016/j.ocemod.2016.10.002

Hormann, V., Centurioni, L. R., Mahadevan, A., Essink, S., D'Asaro, E. A., & Kumar, B. P. (2016). Variability of near-surface circulation and sea surface salinity observed from Lagrangian drifters in the northern Bay of Bengal during the waning 2015 southwest monsoon. *Oceanography*, *29*(2), 124–133. https://doi.org/10.5670/oceanog.2016.45

Kirwan, A. D. (1975). Oceanic velocity gradients. *Journal of Physical Oceanography*, 5(4), 729–735. https://doi.org/10.1175/1520-0485(1975)005(0729:ovg)2.0.co;2

Lévy, M., Klein, P., & Treguier, A.-M. (2001). Impact of sub-mesoscale physics on production and subduction of phytoplankton in an oligotrophic regime. *Journal of Marine Research*, 59(4), 535–565. https://doi.org/10.1357/002224001762842181

Lumpkin, R., & Pazos, M. (2007). Measuring surface currents with surface velocity program drifters: The instrument, its data, and some recent results. In A. Griffa, A. D. KirwanJr., A. J. Mariano, T. Özgökmen, & H. T. Rossby (Eds.), *Lagrangian analysis and prediction of coastal and ocean dynamics* (pp. 39–67). Cambridge University Press. https://doi.org/10.1017/CBO9780511535901.003

Mahadevan, A., & Archer, D. (2000). Modeling the impact of fronts and mesoscale circulation on the nutrient supply and biogeochemistry of the upper ocean. *Journal of Geophysical Research*, 105(C1), 1209–1225. https://doi.org/10.1029/1999JC900216

Mahadevan, A., Jaeger, G. S., Freilich, M., Omand, M. M., Shroyer, E. L., & Sengupta, D. (2016). Freshwater in the Bay of Bengal: Its fate and role in air-sea heat exchange. *Oceanography*, 29(2), 72–81. https://doi.org/10.5670/oceanog.2016.40

Mahadevan, A., Pascual, A., Rundnick, D., Ruiz, S., Tintoré, J., & D'Asaro, E. (2020). Coherent pathways for vertical transport from the surface ocean to interior. *Bulletin of the American Meteorological Society*, 101(11), E1996–E2004. https://doi.org/10.1175/BAMS-D-19-0305.1

Maximenko, N., Lumpkin, R., & Centurioni, L. (2013). Ocean surface circulation. In *International Geophysics* (Vol. 103, pp. 283–304). Elsevier.

McWilliams, J. C. (2016). Submesoscale currents in the ocean. *Proceedings of the Royal Society A: Mathematical, Physical & Engineering Sciences*, 472(2189), 20160117. https://doi.org/10.1098/rspa.2016.0117

McWilliams, J. C., Gula, J., & Molemaker, M. J. (2019). The Gulf Stream north wall: Ageostrophic circulation and frontogenesis. *Journal of Physical Oceanography*, 49(4), 893–916. https://doi.org/10.1175/JPO-D-18-0203.1

Molinari, R., & Kirwan, A. D. (1975). Calculations of differential kinematic properties from Lagrangian observations in the western Caribbean Sea. *Journal of Physical Oceanography*, 5(3), 483–491. https://doi.org/10.1175/1520-0485(1975)005<0483:codkpf>2.0.co;2

Niiler, P. (2001). The world ocean surface circulation. In G. Siedler, J. Church, & J. Gould (Eds.), *Ocean circulation and climate: Observing and modelling the global ocean* (Vol. 77, pp. 193–204). Academic Press. https://doi.org/10.1016/S0074-6142(01)80119-4

Novelli, G., Guigand, C. M., Cousin, C., Ryan, E. H., Laxague, N. J. M., Dai, H., et al. (2017). A biodegradable surface drifter for ocean sampling on a massive scale. *Journal of Atmospheric and Oceanic Technology*, 34(11), 2509–2532. https://doi.org/10.1175/JTECH-D-17-0055.1

Ohlmann, J. C., Molemaker, M. J., Baschek, B., Holt, B., Marmorino, G., & Smith, G. (2017). Drifter observations of submesoscale flow kinematics in the coastal ocean. *Geophysical Research Letters*, 44(1), 330–337. https://doi.org/10.1002/2016gl071537

Okubo, A. (1970). Horizontal dispersion of floatable particles in the vicinity of velocity singularities such as convergences. *Deep Sea Research and Oceanographic Abstracts*, 17(3), 445–454. https://doi.org/10.1016/0011-7471(70)90059-8

Okubo, A., & Ebbesmeyer, C. C. (1976). Determination of vorticity, divergence, and deformation rates from analysis of drogue observations. *Deep Sea Research and Oceanographic Abstracts*, 23(4), 349–352. https://doi.org/10.1016/0011-7471(76)90875-5

Pascual, A., Ruiz, S., Olita, A., Troupin, C., Claret, M., Casas, B., et al. (2017). A multiplatform experiment to unravel meso- and submesoscale processes in an intense front (AlborEx). *Frontiers in Marine Science*, 4, 39. https://doi.org/10.3389/fmars.2017.00039

Poje, A. C., Ozgökmen, T. M., Lipphardt, B. L., Haus, B. K., Ryan, E. H., Haza, A. C., et al. (2014). Submesoscale dispersion in the vicinity of the Deepwater Horizon spill. *Proceedings of the National Academy of Sciences of the United States of America*, 111(35), 12693–12698. https://doi.org/10.1073/pnas.1402452111

Poulain, P.-M. (1993). Estimates of horizontal divergence and vertical velocity in the equatorial Pacific. *Journal of Physical Oceanography*, 23(4), 601–607. https://doi.org/10.1175/1520-0485(1993)023<0601:eohdav>2.0.co;2

Poulain, P.-M., Centurioni, L., Özgökmen, T., Tarry, D. R., Pascual, A., Ruiz, S., et al. (2021). On the structure and kinematics of an Algerian Eddy in the southwestern Mediterranean Sea. *Remote Sensing*, 13(15), 3039. https://doi.org/10.3390/rs13153039

Rudnick, D. L., & Klinke, J. (2007). The underway conductivity–temperature–depth instrument. *Journal of Atmospheric and Oceanic Technology*, 24(11), 1910–1923. https://doi.org/10.1175/JTECH2100.1

Ruiz, S., Claret, M., Pascual, A., Olita, A., Troupin, C., Capet, A., et al. (2019). Effects of oceanic mesoscale and submesoscale frontal processes on the vertical transport of phytoplankton. *Journal of Geophysical Research: Oceans*, 124(8), 5999–6014. https://doi.org/10.1029/2019JC015034

Shcherbina, A. Y., D'Asaro, E. A., Lee, C. M., Klymak, J. M., Molemaker, M. J., & McWilliams, J. C. (2013). Statistics of vertical vorticity, divergence, and strain in a developed submesoscale turbulence field. *Geophysical Research Letters*, 40(17), 4706–4711. https://doi.org/10.1002/grl.50919

Spydell, M. S., Feddersen, F., & Macmahan, J. (2019). The effect of drifter GPS errors on estimates of submesoscale vorticity. *Journal of Atmospheric and Oceanic Technology*, 36(11), 2101–2119. https://doi.org/10.1175/JTECH-D-19-0108.1

Sybrandy, A. L., & Niiler, P. P. (1991). The WOCE/TOGA SVP Lagrangian drifter construction manual. *WOCE Report*, 63, 58.

Tarry, D. R., Essink, S., Pascual, A., Ruiz, S., Poulain, P.-M., Özgökmen, T., et al. (2021). Frontal convergence and vertical velocity measured by drifters in the Alboran Sea. *Journal of Geophysical Research: Oceans*, 126(4), e2020JC016614. https://doi.org/10.1029/2020JC016614

Tintoré, J., Gomis, D., Alonso, S., & Parrilla, G. (1991). Mesoscale dynamics and vertical motion in the Alborán Sea. *Journal of Physical Oceanography*, 21(6), 811–823. https://doi.org/10.1175/1520-0485(1991)021<0811:mdavmi>2.0.co;2

Tintoré, J., Gomis, D., Alonso, S., & Wang, D.-P. (1988). A theoretical study of large sea level oscillations in the Western Mediterranean. *Journal of Geophysical Research*, 93(C9), 10797–10803. https://doi.org/10.1029/JC093iC09p10797

Yu, X., Naveira Garabato, A. C., Martin, A. P., Buckingham, C. E., Brannigan, L., & Su, Z. (2019). An annual cycle of submesoscale vertical flow and restratification in the upper ocean. *Journal of Physical Oceanography*, 49(6), 1439–1461. https://doi.org/10.1175/JPO-D-18-0253.1